

Observation of the Crab Nebula with the ASTRI-Horn telescope in 2022/2023

S. Lombardi,^{a,b,*} F. G. Saturni,^{a,b} L. A. Antonelli,^{a,b} C. Bigongiari,^{a,b} E. Fedorova,^a F. Lucarelli,^{a,b} M. Mastropietro,^a F. Visconti,^{a,b} G. Leto,^c M. Capalbi,^d O. Catalano,^d G. Contino,^d S. Iovenitti,^e D. Mollica,^d R. Z. Sanchez Castelan,^c P. Sangiorgi,^d G. Sironi,^e G. Sottile,^d A. Giuliani,^f S. Scuderi,^f and G. Pareschi^e for the ASTRI Project^g

^aINAF, Osservatorio Astronomico di Roma, Via Frascati 33, I-00078 Monte Porzio Catone (Roma), Italy

^bASI, Space Science Data Center, Via del Politecnico s.n.c., I-00133 Roma, Italy

^cINAF, Osservatorio Astronomico di Catania, Via Santa Sofia 78, I-95123 Catania, Italy

^dINAF, Istituto di Astrofisica Spaziale e Fisica Cosmica, Via Ugo la Malfa 153, I-90146 Palermo, Italy

^eINAF, Osservatorio Astronomico di Brera, Via Brera 28, I-20121 Milano, Italy

^fINAF, Istituto di Astrofisica Spaziale e Fisica Cosmica, Via Alfonso Corti 12, I-20133 Milano, Italy

^g<http://www.astri.inaf.it/en/library/>

E-mail: saverio.lombardi@inaf.it

The Italian National Institute for Astrophysics (INAF) is leading the ASTRI Project, whose main objective in the early years was the design, development and deployment of an end-to-end dual-mirror 4-m diameter prototype of the Cherenkov Telescope Array Observatory (CTAO) small-sized telescopes (SSTs) for gamma-ray astronomy in the 1–200 TeV energy range. The prototype, named the ASTRI-Horn telescope, is located on Mount Etna (Italy) and features innovative solutions, such as a dual-mirror aplanatic optical system and a Cherenkov camera based on silicon photo-multiplier (SiPM) detectors. After achieving in the past years the first optical validation (2017) and the first detection at TeV energies of a gamma-ray source (2018) by a Cherenkov telescope in dual-mirror Schwarzschild-Couder configuration, in recent years (2020–2022) the ASTRI-Horn telescope underwent significant maintenance and refurbishment to restore damaged systems and improve technical performance. The telescope is currently fully operational and carries on different scientific programs, including gamma-ray, cosmic-ray, and muon-radiography of the Etna volcano investigations. In particular, in the period between fall 2022 and spring 2023, a new observing campaign on the Crab Nebula source was carried out to evaluate the new telescope performance. In this contribution, we present the Crab Nebula data sample collected by the ASTRI-Horn telescope in the aforementioned campaign and discuss some preliminary results.

The 38th International Cosmic Ray Conference (ICRC2023)
26 July – 3 August, 2023
Nagoya, Japan



*Speaker. This contribution was made possible by the work of many people. The full list of authors will be included in a forthcoming publication.

1. Introduction

The Italian National Institute for Astrophysics (INAF) is leading the ASTRI (*Astrofisica con Specchi a Tecnologia Replicante Italiana*) Project [1, 2], with primary goal of deploying and operating an array of 4-m class Imaging Atmospheric Cherenkov Telescopes (IACTs) to investigate the 1–200 TeV gamma-ray sky. The array, named ASTRI Mini-Array, is being built at the *Observatorio del Teide* (Tenerife, Spain), in collaboration, among other national and international partners, with the Spanish *Instituto de Astrofisica de Canarias* (IAC). The completion of the full array and the start of regular scientific operations are foreseen in a few years.

The ASTRI Mini-Array telescopes are an evolution of the ASTRI-Horn telescope [3], a prototype developed in the context of the small-sized telescopes (SSTs) of the Cherenkov Telescope Array Observatory (CTAO) [4]. The ASTRI-Horn telescope is located at the INAF “M. C. Fracastoro” observing station in Serra La Nave (Mt. Etna, Italy) and is based on a Schwarzschild-Couder (SC) innovative design, in which the 4.3-m primary mirror (M1) is composed of 18 aluminium-layered segments, while the 1.8-m secondary mirror (M2) is monolithic [5]. The SC configuration allowed to design a compact silicon photo-multiplier (SiPM) Cherenkov camera with a field of view (FoV) greater than $\sim 10^\circ$ in diameter. The ASTRI-Horn camera is composed of 21 Photon Detection Modules (PDMs) each of 8×8 pixels, with a total of 1344 active pixels each with dimensions of $7 \text{ mm} \times 7 \text{ mm}$ [6], reaching an effective FoV of $\sim 7.5^\circ$ in diameter¹.

The ASTRI-Horn telescope was optically validated in 2017 [7]. During a subsequent observing season (2018–2019) the telescope achieved the first detection of the Crab Nebula source by any Cherenkov telescope in a dual-mirror configuration [8]. Successively, between 2020 and 2022, the system underwent a period of major overhaul [3], in which M2 and some panels of M1 were replaced to improve the optical reflectivity of the instrument (see Fig. 1), and the SiPM Cherenkov camera was completely refurbished. A new observing campaign of the Crab Nebula was then carried out. The main aim was to collect data of the “standard candle” for ground-based gamma-ray astronomy to assess the scientific performance of the system, through the derivation of the spectral properties of the source to be compared with those obtained from the main operating IACTs [9–11]. In this contribution, we describe the data collected during the aforementioned campaign and present some preliminary results of the data analysis.

2. Observations

The Cherenkov observations of the Crab Nebula – RA(J2000) = $05^{\text{h}} 34^{\text{m}} 31^{\text{s}}.94$, DEC(J2000) = $+22^\circ 00' 52''.2$ – with the ASTRI-Horn telescope were performed between November 2022 and March 2023. The source was observed in wobble mode [12], with data equally split in two pointing positions (dubbed W1 and W2) located symmetrically at 0.5° from the Crab Nebula position, in order to ensure optimum sky coverage and background estimation. The survey was carried out during dark time at zenith angles in the range from 15° to 40° . The optimal trigger configuration was selected after a dedicated trigger threshold scan performed at the beginning of the campaign. Data were taken with a trigger configuration set to 5 contiguous pixels above a threshold

¹The Cherenkov cameras of the nine ASTRI Mini-Array telescopes will have instead 37 active PDMs [13], for an effective FoV of $\sim 10.5^\circ$ in diameter.

of 8.2 photon equivalent (p.e.) per pixel, resulting in an average data acquisition rate of the order of 25 Hz (for observations in good weather conditions). In total, 33.7 hours of Crab Nebula data (before data selection) were collected. In addition, 12.9 hours of control OFF data (before data selection) were also collected, in which suitable sky regions without any known gamma-ray source in the FoV were observed (immediately before and after the Crab Nebula observations) in the same range of zenith and azimuth angles as the Crab Nebula data. These OFF data were taken for a twofold reason: first, to validate the Monte Carlo simulations needed to perform the complete data reduction and analysis [14], and second, to obtain an independent sample of data to be used for cross-checking the background in the Crab Nebula data.

During the entire observing period, one of the 18 M1 panels was kept covered with an opaque layer because its optimal position could not be adjusted through active mirror control; in addition, two PDMs located at the edge of the Cherenkov camera were kept disabled for technical reasons (see Fig. 1). The combined loss of performance from the nominal condition due to these two hardware issues has not yet been fully quantified, although from a rough estimate it is expected to be less than $\sim 10\%$. In any case, the Crab Nebula and OFF observations were carried out smoothly and the data were properly collected and transferred to the ASTRI Data Center [15].

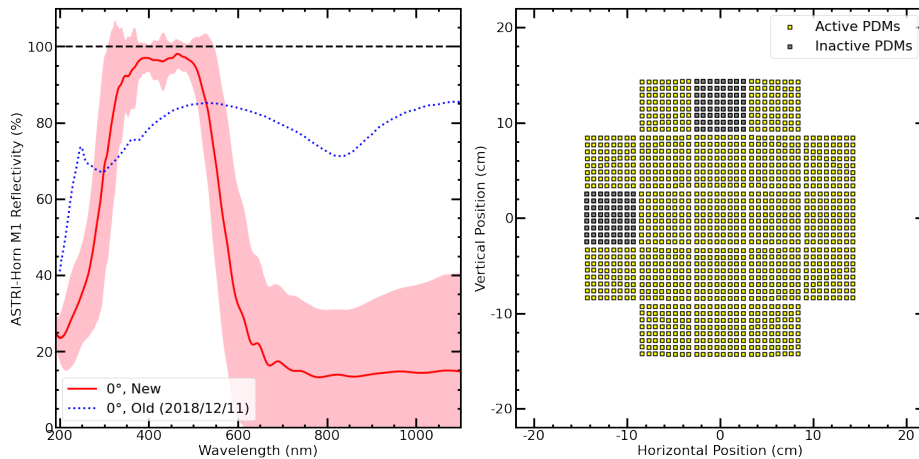


Figure 1: *Left panel:* average ASTRI-Horn M1 reflectivity curve (*red solid line*) with the associated uncertainty at 68% confidence level (*pink area*) as a function of the wavelength (normal incidence only). For comparison, the old average reflectivity curve (*blue dotted line*) is also reported. *Right panel:* ASTRI-Horn camera geometry, with both active (*yellow squares*) and disabled (*grey squares*) PDMs shown.

3. Data reduction and analysis

A preliminary reduction and analysis of the data was performed using the A-SciSoft (ASTRI Scientific Software) package (v0.5.8), the official scientific software of the ASTRI Project [14].

Unfortunately, at the time of writing this work, a full end-to-end analysis of the data up to the generation of the final science products (mainly the spectral energy distribution of the source) has not yet been possible because the simulations [16] necessary for the purpose are still being produced and validated. However, a preliminary analysis was performed to verify the quality of the data at the analysis level and, possibly, identify a hint of gamma-ray signal in the Crab Nebula

data by alternative, albeit largely less performing, methods (see Sec. 4) with respect to the standard ones (which are based on the Random Forest method [17] for event reconstruction). To perform this preliminary analysis, in the absence of appropriate simulations, we made use of the simulated gamma-ray events produced for the 2018–2019 observing campaign. These simulations had been produced through the CoRSiKa [18] and `sim_telarray` [19] software chains, considering the ASTRI-Horn hardware setup in place at that time. The simulations had been reduced with the same processing chain configuration applied to the real data collected in that observing campaign [8]. Specifically, only the low-gain (LG) channel had been used and the standard image cleaning algorithm had been set with thresholds $L1 = 20$ p.e. and $L2 = 10$ p.e.. As a result, in order to take advantage of the 2018–2019 campaign MC simulations, we applied, on a very preliminary basis, the same analysis setup to the data collected in the 2022-2023 data taking campaign.

The raw data, containing the full information available per pixel (integrated signal amplitude in analog-to-digital converter counts) for each triggered shower, were calibrated in order to extract and convert the signal into p.e. by applying conversion coefficients derived from specific camera calibration data through a dedicated calibration software [20]. In this step, the response of each camera pixel was equalized through the application of suitable flat-field [21] and cross-talk correction factors [13]. After the calibration step, the standard two-thresholds two-pass image cleaning algorithm [8] implemented in the ASTRI pipeline was applied to the data, with same thresholds as the data reduction of 2018–2019 data samples, as already mentioned. After this step, a parameterization of each cleaned image was performed. The computed parameters are mainly based on the moments up to the third order of the light distribution on the camera [22]. In this step the telescope pointing direction and the source position in camera coordinates were also extracted from dedicated ancillary data and linked to each shower image. In particular, for the source position determination we made use of a novel technique based on the astrometry of the variance data collected simultaneously to the scientific data. This technique has proven suitable in revealing possible target mispointings and correcting them. More details can be found in [23].

For each observing night, we performed a (preliminary) data selection taking into account quality checks at different levels:

- the rejection of data affected by technical problems, such as instabilities in the pedestals and signals of the camera PDMs;
- the removal of data showing large fluctuations in the trigger rate and/or taken with bad atmospheric conditions (monitored through a dedicated weather station system and an all-sky camera);
- the exclusion of data with Cherenkov image rate outside a 30% stability at analysis level (specifically after the application of the image cleaning procedure).

In total, 24.6 hours of Crab Nebula data were selected ($\sim 70\%$ of the total) following the above criteria. It is worth mentioning that most of the data were rejected due to bad weather conditions during data taking rather than to hardware issues. Fig. 2 shows the mean rates (after cleaning procedure) and zenith angles of the selected Crab Nebula runs.

Once the events were cleaned, parameterized, and selected, we conducted a preliminary search of gamma-ray signal in the collected data by applying to them *static cuts* based on a specific set

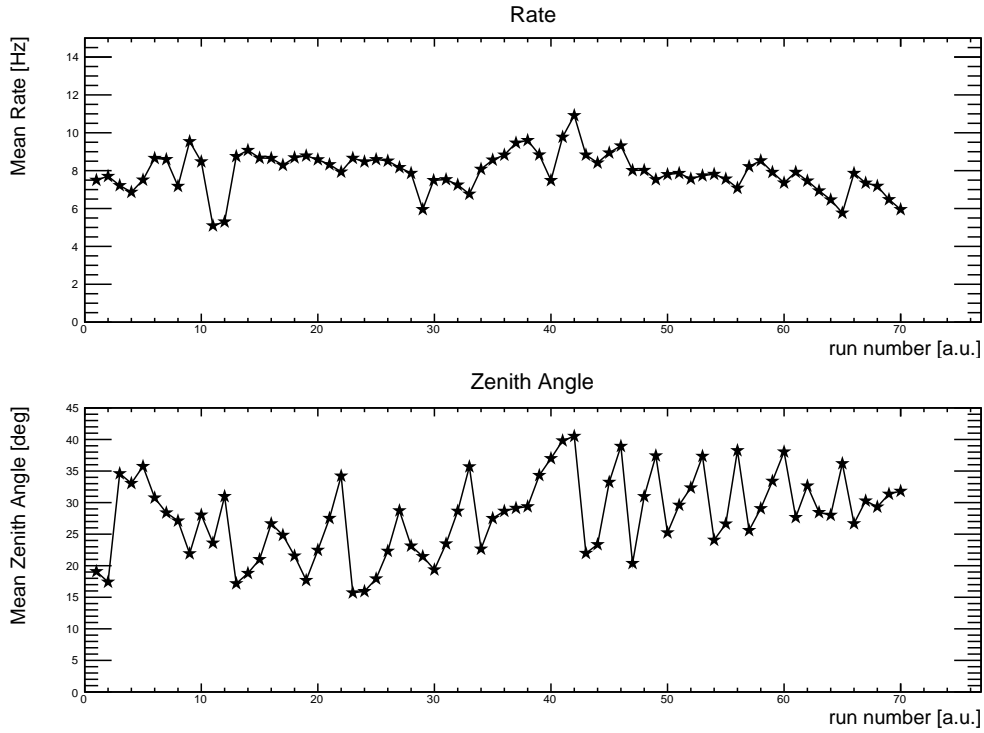


Figure 2: Mean rates (after the application of the image cleaning procedure, with thresholds $L1 = 20$ p.e. and $L2 = 10$ p.e.) (*top panel*) and mean pointing zenith angles (*bottom panel*) of the selected Crab Nebula data runs.

of Hillas parameters. To define these static cuts, we made use of the MC gamma-ray data sample produced during the 2018–2019 campaign and a selected sample of real OFF data taken in the 2022–2023 campaign. First, we binned events of both samples in 2D-bins of $\log_{10}(S)$ and D , where S and D stand for the Hillas parameter Size (total content in p.e. of the image) and Dist (distance from the image center of gravity to the source position), respectively. Then, in each 2D-bin², we produced the binned normalized distributions of the image parameters Width (W), Length (L), Concentration (C), and the module of Asymmetry ($|A|$)³ [22] of the MC gamma-ray and real OFF images. Since the MC simulated events were generated considering a (true) energy power-law of index $\Gamma = -2$ (to increase the statistics of simulated events at the highest energies), each MC event was properly reweighed to match the power-law distribution of the expected real gamma-ray excesses (i.e., an index of -2.6 [24]).

Once all distributions were produced, for each Hillas parameter $p = \{W, L, C, |A|\}$ in each 2D-bin, we combined the distributions of MC and real OFF events into a quality factor Q defined as follows:

$$Q(p|\mathbf{H}) = \frac{N_{\text{on}}(p|\mathbf{H}) - N_{\text{off}}(p|\mathbf{H})}{\sqrt{N_{\text{on}}(p|\mathbf{H}) + N_{\text{off}}(p|\mathbf{H})}}, \quad (1)$$

²We considered four linear bins in $\log_{10}(S)$, from 2.5 to 4.5, and four bins in D , from 0° to 4° .

³These (source-independent) image parameters were chosen based on the gamma/background separation power found in the data analysis of the 2018–2019 campaign.

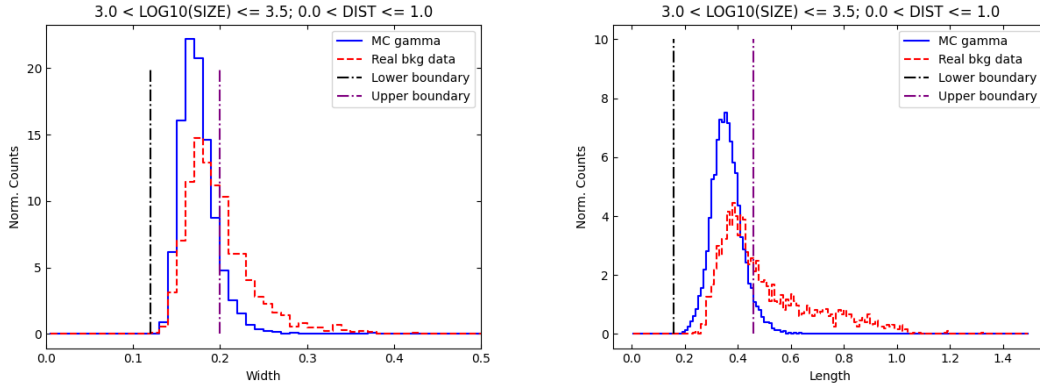


Figure 3: *Left panel:* MC gamma-ray (blue solid line) and real OFF (red dotted line) distributions of the parameter W in one of the 2D-bin in $\log_{10}(S)$ and D , along with the corresponding static cuts (dot-dashed lines) that maximize the quality factor Q (see text). *Right panel:* equivalent distributions and static cuts for the parameter L , in the same 2D-bin.

where $N_{\text{on}}(p|\mathbf{H})$ is the sum of the distributions of MC gamma-rays and real OFF events in each 2D-bin belonging to the set of events \mathbf{H} that starts from (or end up to) a certain value of p , and $N_{\text{off}}(p|\mathbf{H})$ is the equivalent definition taking into account real OFF data only. Finally, we identified the values of each parameter p that best separated the MC gamma-ray distribution from the real OFF distribution by maximizing the values of $Q(p|\mathbf{H})$: this was done for both increasing and decreasing cumulative distributions, in order to find a lower and higher bound for each p to be used as static cut for the gamma/hadron separation. In this maximization process, to prevent the inclusion of bins in which a low event count was accidentally causing the quality factor to diverge, we also requested that the process should stop when 95% of MC gamma-ray counts were included into the calculation of $N_{\text{on}}(p|\mathbf{H})$. At the end of this procedure we obtained the set of static cuts (for each of the Hillas parameters W , L , C and $|A|$, and for each considered 2D-bin) that best discriminated between MC gamma-rays and real background. In Fig. 3, we show two examples of static cut determination obtained with this procedure.

4. Preliminary results

In order to search for a gamma-ray excess in the data we made use of the so-called $|\text{Alpha}|$ -plot, that is we compared the distribution of the module of the Alpha parameter⁴ calculated toward the on-source position (ON distribution) with the distribution calculated considering a suitable off-source position (OFF distribution) with the same angular acceptance as the on-source position. Since the data were taken in wobble mode [12], we could use off-source positions (five, in our case) extracted from the same Crab Nebula data.

⁴Alpha is the angle between the major axis of the recorded image and the vector connecting its center of gravity with the source position in the camera plane. Gamma-ray shower images from the source tend to point with their major axes toward the source position in the camera (showing hence a distribution peaked at low Alpha values), whereas images of background showers do not show any preferred orientation, having isotropic arrival directions (showing thus an almost flat Alpha distribution).

The resulting $|\text{Alpha}|$ -plot, after the application of the static cuts described in Sec. 3, is shown in Fig. 4. We found a clear hint of signal with 195 ± 47 excess events within a fiducial $|\text{Alpha}|$ signal region of 10° , corresponding to a significance of 4.3 standard deviations (σ) calculated according to Eq. 17 of [25]. We stress that this preliminary result cannot be directly compared with that obtained in the 2018–2019 campaign [8] because it was achieved with a sub-optimal procedure compared with the standard one adopted for the 2018–2019 data analysis.

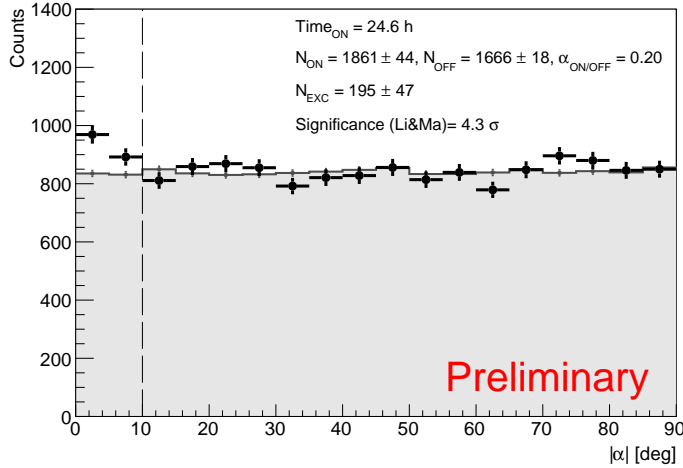


Figure 4: $|\text{Alpha}|$ -distributions of the Crab Nebula (ON, black) and the background (OFF, grey) events from ASTRI-Horn observations taken between November 2022 and March 2023, after the application of static cuts in the parameters W , L , C , and $|A|$ (see text). The region between zero and the vertical dashed line (at 10°) represents the fiducial signal region.

5. Summary and outlook

In this contribution, we described the new observing campaign on the Crab Nebula conducted with the ASTRI-Horn telescope in 2022–2023. Compared with the previous observing campaign in 2018–2019, which resulted in the firm detection of the source, the system has been completely renewed. It is therefore expected to perform better in terms of both hardware stability and scientific performance.

Although a complete analysis of the new collected data was not possible due to the unavailability of appropriate simulations that are still being produced and validated, we performed a preliminary analysis to check the quality of the data and to search for a hint of gamma-ray signal in the collected data, using a rather basic (but partially independent of the necessary simulations) procedure. The preliminary results are certainly sub-optimal, and we expect that with the complete and validated set of MC simulations we will be able not only to increase the significance of the gamma-ray signal to a robust detection, but also to push the analysis as far as obtaining a spectral characterization of the source.

Nevertheless, the hint of signal that we obtained from the preliminary analysis presented in this work goes in the direction of proving that the new system performs adequately. We look forward

to the availability of the complete set of MC simulations to conduct a more thorough analysis and obtain more robust results, with the final aim to achieve the scientific validation of the system.

Acknowledgments

This work was conducted in the context of the ASTRI Project. We gratefully acknowledge support from the people, agencies, and organisations listed here: <http://www.astri.inaf.it/en/library/>. We acknowledge financial support from the ASI-INAF agreement n. 2022-14-HH.0. This paper went through the internal ASTRI review process.

References

- [1] S. Scuderi *et al.*, *JHEAp* **35**, 52 (2022).
- [2] A. Giuliani *et al.*, Proc. 38th ICRC (Nagoya, Japan), PoS(ICRC2023)892 (2023).
- [3] G. Leto *et al.*, Proc. 38th ICRC (Nagoya, Japan), PoS(ICRC2023)729 (2023).
- [4] G. Tagliaferri *et al.*, Proc. SPIE **12182**, 121820K (2022).
- [5] R. Canestrari *et al.*, Proc. SPIE **9603**, 960303 (2015).
- [6] O. Catalano *et al.*, Proc. SPIE **10702**, 1070237 (2018).
- [7] E. Giro *et al.*, *A&A* **608**, A86 (2017).
- [8] S. Lombardi *et al.*, *A&A* **634**, A22 (2020).
- [9] MAGIC Coll., *JHEAp* **5**, 30 (2015).
- [10] VERITAS Coll., PoS **236**, 792 (2016).
- [11] M. Holler *et al.*, PoS **236**, 847 (2016).
- [12] V. P. Fomin *et al.*, *Astropart. Phys.* **2**, 151 (1994).
- [13] D. Mollica *et al.*, Proc. 38th ICRC (Nagoya, Japan), PoS(ICRC2023)765 (2023).
- [14] S. Lombardi *et al.*, Proc. SPIE **10707**, 107070R (2018).
- [15] S. Lombardi *et al.*, Proc. 38th ICRC (Nagoya, Japan), PoS(ICRC2023)682 (2023).
- [16] F. G. Saturni *et al.*, Proc. 38th ICRC (Nagoya, Japan), PoS(ICRC2023)719 (2023).
- [17] L. Breiman, *Mach. Learn.* **45**, 5 (2001).
- [18] D. Heck *et al.*, *CORSIKA: a Monte Carlo code to simulate extensive air showers*, TIB Hannover (1998).
- [19] K. Bernlöhner, *Astropart. Phys.* **30**, 149 (2008).
- [20] T. Mineo *et al.*, Proc. 38th ICRC (Nagoya, Japan), PoS(ICRC2023)733 (2023).
- [21] G. Contino *et al.*, Proc. 38th ICRC (Nagoya, Japan), PoS(ICRC2023)739 (2023).
- [22] A. M. Hillas, Proc. ICRC1985 **3**, 445 (1985).
- [23] S. Iovenitti *et al.*, Proc. 38th ICRC (Nagoya, Japan), PoS(ICRC2023)836 (2023).
- [24] F. Aharonian *et al.*, *ApJ* **614**, 2 (2004).
- [25] T.-P. Li & Y.-Q. Ma, *ApJ* **272**, 317 (1983).